

## **ACKNOWLEDGMENT**

I would like to express our heartfelt gratitude to **Dr. Sangram Roy**, Department of Chemical Engineering, Birla Institute of Technology, Mesra, for his invaluable guidance, unwavering support, and insightful suggestions throughout the duration of our project, "**CFD Modelling for ethanol steam reforming for production of hydrogen in COMSOL**". His expertise and encouragement have inspired us to tackle challenges with confidence and have significantly contributed to the successful completion of this work. I sincerely thank **Dr. Siddhartha Mukherjee**, IIT Guwahati, for his invaluable guidance in learning COMSOL from the ground up and for his constant support in resolving functional issues and clarifying core concepts throughout the project. I am also sincerely grateful to the **Computer Laboratory team** and the **Chemical Engineering Department staff** at **BIT Mesra** for providing technical support and assistance in carrying out the computational simulations essential to this project. Their timely help and cooperation greatly facilitated our research efforts.

The conducive learning environment and access to laboratory facilities have been pivotal in ensuring the smooth progression of this project. We extend our sincere appreciation to all the faculty and staff members of the Department of Chemical Engineering for their timely assistance, encouragement, and constructive feedback, which helped us refine our ideas and methods at every stage of the project. We would also like to acknowledge the contributions of researchers and authors whose prior work served as a foundation and inspiration for our study. This project has been a profound learning experience, and we are thankful to everyone who played a role in its successful completion.

## ABSTRACT

This project presents a modelling-based study of ethanol steam reforming for hydrogen production, with a focus on improving efficiency through electrification. A series of simulations were conducted using COMSOL Multiphysics to analyze how process parameters such as temperature and pressure influence hydrogen yield. The study begins by validating the model against existing literature, ensuring that the approach is both accurate and reliable. Although differences in reactor geometry—1D in our case versus 3D in the reference study—led to some variation in species profiles, the final concentrations showed strong alignment.

A maximum hydrogen yield of approximately 80% was achieved at 1150 K, 4 bar pressure, and an S:C ratio of 3:1, highlighting the favourable conditions for efficient hydrogen production. Additionally, extending the model to 2D with applied heat flux showed a further increase in hydrogen yield, demonstrating the positive effect of direct energy input on reaction performance. In an effort to explore sustainable alternatives to conventional heating, the concept of ohmic heating was integrated into the model. Inspired by recent advancements in microwave-assisted reforming, this approach offers a promising route for energy-efficient hydrogen production. The results highlight that both higher temperatures and pressures contribute positively to hydrogen yield, and electrification may serve as a practical enhancement for reforming processes. This study lays the groundwork for future research in low-carbon hydrogen generation using renewable electricity.

## INDEX

S. No.	Title	Page no.
1.	Introduction	7
2.	Literature review	9
3.	Objective of work	10
4.	Methodology	10
4.1	Reformer Configuration	10
4.2	CFD Model	11
4.3	Modules	14
4.4	Cases studied	16
5.	Results & discussions	17
5.1	1D – Non-dimensional and dimensional	17
5.2	1D - Validation of the results	20
5.3	2D – Without heat flux	22
5.4	2D – With heat flux (100 & 500 W/m <sup>2</sup> )	23
5.5	2D – With ohmic heating	24
6.	Conclusion & Future Work	25
7.	References	26

## 1. INTRODUCTION

In recent years, hydrogen has emerged as one of the most promising solutions in the global push toward a cleaner, more sustainable energy future. Often referred to as the "fuel of the future," hydrogen stands out because of its exceptionally high energy density—120 MJ per kilogram—and its ability to produce zero emissions at the point of use. These features make it an ideal candidate to help the world transition away from carbon-intensive fuels and toward low-emission energy systems.

Yet, hydrogen is not without its hurdles. The widespread adoption of hydrogen faces three primary challenges:

- First, infrastructure for hydrogen storage, transport, and refuelling is still underdeveloped, especially compared to traditional energy carriers like oil and natural gas.
- Second, production costs remain high, largely due to the energy-intensive processes involved in generating hydrogen through conventional means.
- Third, the scalability of hydrogen technologies—from electrolysis to carbon capture—is still evolving, creating uncertainty in meeting large-scale demand.

What we are witnessing now can aptly be described as a "hydrogen gold rush." In 2020, fewer than a dozen companies were seriously investing in natural hydrogen exploration—a clean form of hydrogen that naturally seeps from the Earth's crust. Fast forward to 2023, and over 40 companies have joined the race. Excitement is growing around the possibility that natural hydrogen could meet the world's energy demands for centuries—and at an estimated production cost of less than \$1 per kilogram.

However, this promising field is still in its early stages, and until it matures and becomes commercially viable, we must continue to develop and optimize alternative hydrogen production routes, such as steam reforming, electrolysis, and biomass gasification.

### The Colour Code of Hydrogen: A Spectrum of Sustainability

Hydrogen is often categorized by colours, which indicate how it is produced and how environmentally friendly that process is. Each type has different implications for carbon emissions and cost:

Table 1: Hydrogen Colour Spectrum [5]

Type	Production Method	Global share	Estimated Cost (USD/kg)
Brown/Black	Coal	19%	0.7-2.3
Gray	Natural gas	62%	1.3-2.5
Blue	Natural gas with carbon capturing	0.7%	-
Green	Water electrolysis using renewable electricity	0.04%	-

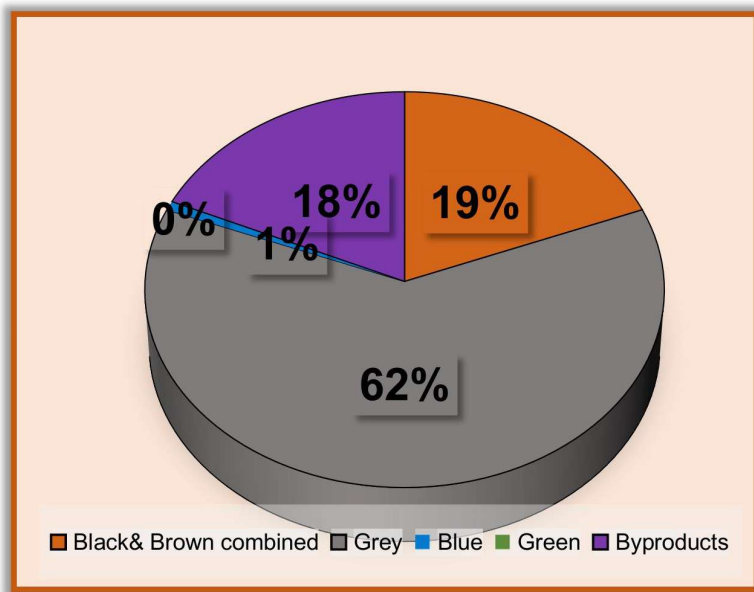


**Fig 1: The H<sub>2</sub> Colour Spectrum**

Beyond being a clean fuel, hydrogen is playing a transformational role across various deep-tech domains, both directly and indirectly. Some of its most impactful applications include:

- Quantum Computing: Used in cryogenics for superconducting processors.
- Artificial Intelligence & Machine Learning: Powering green data centres through hydrogen fuel cells.
- Space Exploration: A critical component in rocket propulsion and onboard energy systems.
- Robotics: Extending the operating time of mobile autonomous robots, fuel Cells for endurance in drones, underwater robots.
- Semiconductors & Photonics: Supporting high-purity processes in chip fabrication. In semiconductors, hydrogen is used in plasma etching, chemical vapour deposition and in photonics, hydrogen is used in glass fibre protection, optical coating processes.
- Clean Energy Systems: Enabling energy storage, grid balancing, and hydrogen-powered transport solutions.

Its versatility, abundance, and environmental benefits have positioned hydrogen as a cornerstone of next-generation technology and sustainability initiatives. Ethanol, a renewable biofuel derived from biomass fermentation, serves as a promising feedstock for hydrogen production due to its high hydrogen content, ease of handling, and widespread availability. The work employs a multiphysics simulation framework in COMSOL to analyze the kinetic behaviour of sequential reactions in ESR, including ethanol decomposition, water-gas shift, and methane steam reforming. This computational approach enables deeper insights into reaction dynamics and aids in optimizing conditions for maximum ethanol conversion and hydrogen yield.

## 2. LITERATURE REVIEW

S.No	Ref	Reformer Type	Feed Type	Operating Conditions				Conversion	H2 Yield
				T(K)	P	Feed flow rates	Catalyst		
1	Cifuentes, A., Torres, R., & Llorca, J. (2020).	Cordierite Honeycomb	Ethanol, Steam	1150	4 bar	S:C=3:1	Rh-Pd/CeO <sub>2</sub>	100%	80%
2	Sidhu, T. P. K., Govil, A., & Roy, S. (2017).	Monolithic	Ethanol , Steam	873	-	S:C=6:1	Ni/CeO <sub>2</sub> /ZrO <sub>2</sub>	40-81% (81% combustion counter flow)	-
3	Hakim, L., Yaakob, Z., Ismail, M., Daud, W. R. W., & Sari, R. (2013).	Tubular Fixed Bed Microreactor	Glycerol, Water	873	1 atm	W:G= 8:1	Ni-Ce-Cu supported on hydroxyapatite	97.3%	57.5%
4	Fakeeha, A., Ibrahim, A. A., Aljuraywi, H., Alqahtani, Y., Alkhodair, A., Alswaidan, S., ... & Al-Fatesh, A. S. (2020).	Tubular Fixed Bed Microreactor	Methane , Oxygen, Nitrogen	923	1 atm	M:O:N = 6:3:4	10% Ni on $\gamma$ -Al <sub>2</sub> O <sub>3</sub>	90 %	72 %
5	US8075869B2	Microwave assisted catalytic reformer	Methane	873-973	1 atm	120 ml/min	nickel oxide (NiO) supported on aluminum oxide	20-30%	20-30%

(Al<sub>2</sub>O<sub>3</sub>). |

The first two studies in the literature survey use COMSOL Multiphysics for numerical modelling with ethanol and steam as feedstocks. They vary from one another, though, in terms of the feed flow conditions and the catalysts used. The following two articles provide useful performance comparison benchmarks based on experimental studies that investigate ethanol conversion and hydrogen production using different feedstocks. The last entry is a patent for a microwave-assisted catalytic reformer, which uses microwave energy to heat the catalyst particles directly, increasing the process's energy efficiency. Motivated by this, we are working to improve hydrogen yield during ethanol steam reforming by using ohmic (Joule) heating. Although there have been attempts to electrify this region, there are currently few thorough studies that concentrate exclusively on ohmic heating in ethanol steam reforming.

### **3. OBJECTIVE OF WORK**

Design a hydrogen reformer using ethanol as the feedstock:

- Analyze the effect of the Damköhler number (Da) on hydrogen yield
- Evaluate maximum yield of hydrogen in 1D
- Evaluate hydrogen production under both adiabatic and externally heated conditions in 2D

### **4. Methodology**

#### **4.1 Reformer configuration**

The reformer configuration in this study was modeled in both one-dimensional (1D) and two-dimensional (2D) geometries using COMSOL Multiphysics to simulate the ethanol steam reforming process. A tubular reactor was considered, representative of a packed-bed catalytic reformer, where the catalyst was assumed to be uniformly distributed across the reactor domain. For the 1D model, the reactor was simplified as an axial domain to capture the variation of species concentrations and temperature along the reactor length. In contrast, the 2D model accounted for both axial and radial variations, enabling a more detailed analysis of transport phenomena such as diffusion and heat transfer within the catalyst layer.

Catalyst loading was assumed to be evenly dispersed, with the active catalytic phase comprising a Rh-Pd/CeO<sub>2</sub> formulation based on literature data. While actual catalyst synthesis and coating procedures were not physically implemented in this simulation, catalyst properties such as porosity, particle size, and reaction kinetics were incorporated through appropriate boundary conditions and rate expressions. Thermophysical and transport properties of all species involved were obtained from COMSOL's built-in thermodynamics database to ensure realistic and consistent behaviour across simulations.



Fig 2: Monolith Channel

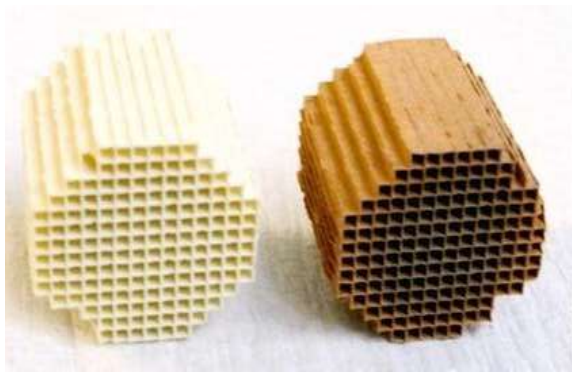


Fig 3: Honeycomb Cordierite

The feed stream, composed of ethanol and water at a steam-to-carbon ratio of 3:1, was introduced at the reactor inlet as a gaseous mixture. No carrier gas was used. The simulation tracked the evolution of key gas-phase species (ethanol, CH<sub>4</sub>, CO, CO<sub>2</sub>, H<sub>2</sub>, and H<sub>2</sub>O) through the reactor using experimentally derived kinetic rate constants for each reaction step. Plug-flow boundary conditions were applied at the inlet, while the outlet was modeled with a convective flux to simulate free exit. Mass conservation and trends in conversion and hydrogen yield were verified to align with data reported in relevant experimental studies.

#### 4.2 CFD Model

A non-isothermal CFD model was developed using COMSOL Multiphysics 6.0 to simulate hydrogen production in both 1D and 2D reactor geometries. The 1D model represented a 1-meter-long catalytic reactor, while the 2D model depicted a rectangular steel reactor (4 m × 1 m) containing internal monolith channels. The finite element method was employed to solve the governing equations, using the PARDISO direct solver for efficient and stable convergence. Simulations were performed on a system with a 12th Gen Intel(R) Core (TM) i7-12700 processor (2.10 GHz), 16 GB of installed RAM, and a 64-bit operating system.

The following assumptions were applied in the CFD models: (i) the gas mixture was considered ideal with Newtonian flow behaviour, (ii) the system operated under steady-state conditions, (iii) steam acted as a solvent in diffusion transport, (iv) inertial terms in the Navier-Stokes equations were neglected, (v) thermal viscous dissipation was ignored, (vi) surface reactions occurred exclusively on the catalyst surface, and (vii) conductive heat transfer within the catalyst layer was approximated to match that of the cordierite support. Additionally, for both 1D and 2D geometries, the inlet velocity was applied only in a single direction.

### Governing Equations (dimensional form):

$$\frac{\partial C_E}{\partial t} + u \frac{\partial C_E}{\partial z} + \eta(1-\varepsilon) C_E C_S k_0 e^{-E/RT} = 0 \quad 1$$

$$\frac{\partial C_S}{\partial t} + u \frac{\partial C_S}{\partial z} + 3\eta(1-\varepsilon) C_E C_S k_0 e^{-E/RT} = 0 \quad 2$$

$$\frac{\partial C_H}{\partial t} + u \frac{\partial C_H}{\partial z} - 6\eta(1-\varepsilon) C_E C_S k_0 e^{-E/RT} = 0 \quad 3$$

$$\frac{\partial C_C}{\partial t} + u \frac{\partial C_C}{\partial z} - 2\eta(1-\varepsilon) C_E C_S k_0 e^{-E/RT} = 0 \quad 4$$

$$\rho \left( \frac{\partial u}{\partial t} + u \frac{\partial u}{\partial x} \right) = - \frac{\partial p}{\partial x} + \mu \left( \frac{\partial^2 u}{\partial x^2} \right) + F \quad 5$$

$$\rho C_p \left[ \frac{\partial T}{\partial t} + u \frac{\partial T}{\partial z} \right] - \eta(1-\varepsilon) C_E C_S k_0 e^{-E/RT} \sum \Delta H = 0 \quad 6$$

E: Ethanol, S: Steam, H: Hydrogen, C: Carbon Dioxide.

The dimensional equations have been transformed into a non-dimensional form through the application of variable scaling. The scaled variables are mentioned below:

$$\tilde{C}_E = \frac{C_E}{C_{E0}}, \quad \tilde{C}_S = \frac{C_S}{C_{E0}}, \quad \tilde{C}_H = \frac{C_H}{C_{E0}}, \quad \tilde{C}_C = \frac{C_C}{C_{E0}}$$

$$\xi = \frac{z}{L_b}, \quad \zeta = \frac{tu}{L_b}, \quad \beta = \frac{(-\Delta H) C_E^\theta}{\rho C_p T_0}, \quad \Theta = \frac{(T-T_0)}{T_0}, \quad \gamma = \frac{Ea}{RT_0}$$

Damköhler Number ( $D_a$ ) is defined as the ratio of rate of chemical reaction to rate of convection.

$$Da = \frac{k_d L_b C_E^\theta}{u}$$

### Governing Equations (non-dimensional form):

$$\frac{\partial \tilde{C}_E}{\partial \zeta} + \frac{\partial \tilde{C}_E}{\partial \xi} + Da \tilde{C}_E \tilde{C}_s \eta(1-\varepsilon) e^{-\gamma/1+\theta} = 0 \quad 1$$

$$\frac{\partial \tilde{C}_S}{\partial \zeta} + \frac{\partial \tilde{C}_S}{\partial \xi} + 3Da \tilde{C}_E \tilde{C}_s \eta(1-\varepsilon) e^{-\gamma/1+\theta} = 0 \quad 2$$

$$\frac{\partial \tilde{C}_H}{\partial \zeta} + \frac{\partial \tilde{C}_H}{\partial \xi} - 6Da \tilde{C}_E \tilde{C}_s \eta(1-\varepsilon) e^{-\gamma/1+\theta} = 0 \quad 3$$

$$\frac{\partial \tilde{C}_C}{\partial \zeta} + \frac{\partial \tilde{C}_C}{\partial \xi} - 2Da \tilde{C}_E \tilde{C}_s \eta(1-\varepsilon) e^{-\gamma/1+\theta} = 0 \quad 4$$

$$\frac{\partial \theta}{\partial \zeta} + \frac{\partial \theta}{\partial \xi} - Da \tilde{C}_E \tilde{C}_s \eta(1-\varepsilon) \beta e^{-\gamma/1+\theta} = 0 \quad 5$$

## Initial & boundary conditions

- At z=0,  $C_E = 10 \text{ mol/m}^3$ ,  $C_S = 30 \text{ mol/m}^3$  (S:C=3:1),  $u = 0.18 \text{ m/s}$
- At t=0,  $C_E = C_S = C_H = C_M = C_{CO} = C_{CO_2} = u = 0$
- At  $\xi=0$ ,  $\tilde{c}_E=1$ ,  $\tilde{c}_S=3$ ,  $\Theta=2.0$
- At  $\tau=0$ ,  $\tilde{c}_E = \tilde{c}_S = \tilde{c}_H = \tilde{c}_M = \tilde{c}_{CO} = \tilde{c}_{CO_2} = \Theta = 0$

## Rate Equations

Although there are many reactions that occur when ethanol is steam-reformed, this study concentrates on three main ones: the Water-Gas Shift Reaction (b), Methane steam reforming (c), and Ethanol Decomposition (a). Because of their dominance in the overall reaction kinetics and suitability for process design and optimization, these reactions were chosen. But the Reverse Water-Gas Shift Reaction can also proceed to a considerable degree at such high temperatures, increasing the production of carbon monoxide. According to earlier research [8,13,17], ethanol first decomposes at lower temperatures over Rh-Pd/CeO<sub>2</sub> catalysts into hydrogen, methane, and carbon monoxide. The Water-Gas Shift (WGS) reaction comes next, and methane then goes through steam reforming at higher temperatures.

Table 3: Kinetic-Thermodynamic reaction data (Cifuentes et al., 2020)

Reactions	Rate Equation	$\Delta H_{298}$
<i>Ethanol Decomposition</i>	$r_1 = k_1 C_E$	49 kJ/mol
<i>Water Gas shift reaction</i>	$r_2 = k_2 C_{CO} C_S - \frac{k_2 C_{CO_2} C_H}{K_2}$	- 41.2 kJ/mol
<i>Methane steam Reforming</i>	$r_3 = k_3 C_M C_S^2 - \frac{k_3 C_{CO_2} C_H^4}{K_3}$	165.1 kJ/mol

Table 4: Reaction kinetics parameters (Sidhu et al., 2017)

Reaction	Frequency Factor		Activation Energy	
	( $m^{3n} mol^{(1-n)} / s m_{cat}^3$ )		(J/mol)	
	Forward	Backward	Forward	Backward
Ethanol Decomposition	1.7*10 <sup>9</sup>		149400	
Water Gas shift	1.4*10 <sup>7</sup>	1.3*10 <sup>4</sup>	124600	76500
Methane steam reforming	5.922*10 <sup>9</sup>	4.358*10 <sup>2</sup>	209200	243900

#### 4.3 Models used in COMSOL

COMSOL Multiphysics was used for the computational modelling, which used a set of physics interfaces to capture the reactor system's Multiphysics behaviour. To resolve the velocity field inside the reactor, the **Laminar Flow** module was first added to the specified geometry. This interface, appropriate for low Reynolds number conditions, solves the momentum conservation equations (see Eq. v) assuming incompressible and Newtonian flow. The complete Navier-Stokes equations reduce to a simplified form, representing creeping flow conditions, because of the low velocity and minimal inertial effects assumed in the system.

The **Heat Transfer in Fluids** module was then added to model the energy transfer involved in conduction and fluid motion. This module works in conjunction with the velocity field obtained from the Laminar Flow interface and solves the energy conservation equation (refer to Eq. vi), enabling accurate prediction of the temperature profile.

The **Chemistry** module was used to define and calculate the reaction kinetics for all chemical reactions that were taken into consideration prior to the inclusion of species transport. The reaction data and kinetic parameters were taken from reliable sources in the literature. This module made it possible to compute local reaction rates, which were subsequently coupled to the ensuing transport and energy equations.

To take into consideration the spatial distribution and transport of chemical species, the **Transport of Diluted Species (TDS)** module was subsequently included. It incorporates convection, diffusion, and reaction terms into the solution of the mass balance equations (Eqs. 1–5). To guarantee precise species transport influenced by both reaction rates and fluid flow, this module was closely integrated with the Chemistry and Laminar Flow modules.

The **Ohmic Heating** (Almind et al., 2020) module was added in the last step to mimic Joule heating and supply the reactor with extra thermal energy via electrical input. In order to align the simulation with sustainable energy practices, it was assumed that this energy source came from renewable electricity. The Electric Currents and Heat Transfer in Solids modules are inherently coupled by the Ohmic Heating interface, enabling the simultaneous computation of thermal and electrical fields. Steel was designated as the reactor body in the Heat Transfer in Solids module in order to appropriately reflect its material properties and thermal conductivity.



Fig 4: **Ohmic Heating in a Monolithic Reactor**

To ensure proper interaction among the different physics interfaces, the **Multiphysics** feature of COMSOL was employed for comprehensive coupling. The following multiphysics couplings were activated:

- **Non-Isothermal Flow**, to couple the Heat Transfer and Laminar Flow modules
- **Diluted Species in Creeping Flow**, to enable consistent coupling between species transport and flow in low Reynolds number regimes
- **Electromagnetic Heating**, to account for the interaction between electrical heating (Ohmic Heating) and solid heat conduction

#### 4.4 Cases Studied

Table 5: Cases Studied

1D	Non dimensional	Effect of $D_a$	$D_a = 0, 1, 10$
	Dimensional	Effect of Temperature	$T = 773K, 823K, 873K, 923K, 950K, 1050K, 1150K$
2D	Temperature  (Stationary and Time dependent)	Without heat flux	Heat Flux= $100W/m^2$
		With $100 W/m^2$ heat flux	Electric Potential= $10V$
		With Ohmic Heating	Reactor Body: Steel
	Ethanol  (Stationary and Time dependent)	Without heat flux	Heat Flux= $100W/m^2$
		With $100 W/m^2$ heat flux	Electric Potential= $10V$
		With Ohmic Heating	Reactor Body: Steel
	Hydrogen  (Stationary and Time dependent)	Without heat flux	Heat Flux= $100W/m^2$
		With $100 W/m^2$ heat flux	Electric Potential= $10V$
		With Ohmic Heating	Reactor Body: Steel

## 5. RESULTS & DISCUSSION

### 5.1 Non-Dimensional

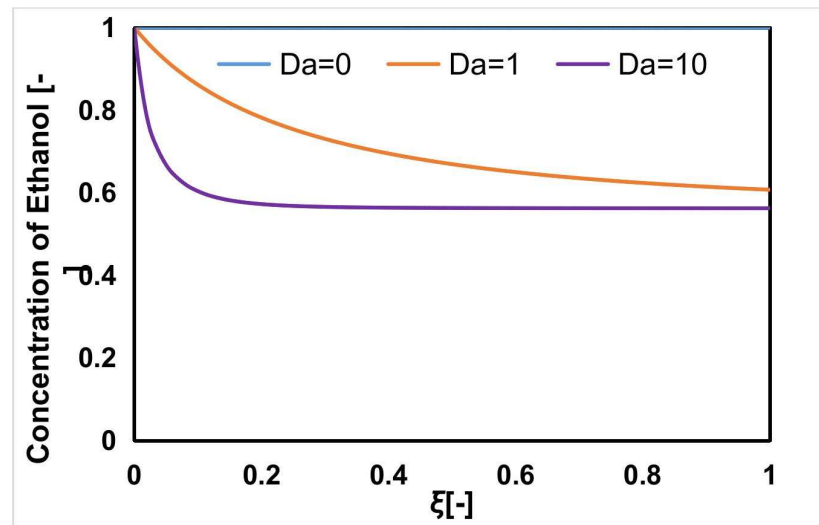


Fig 5: Non-dimensional Concentration vs Non-dimensional Length

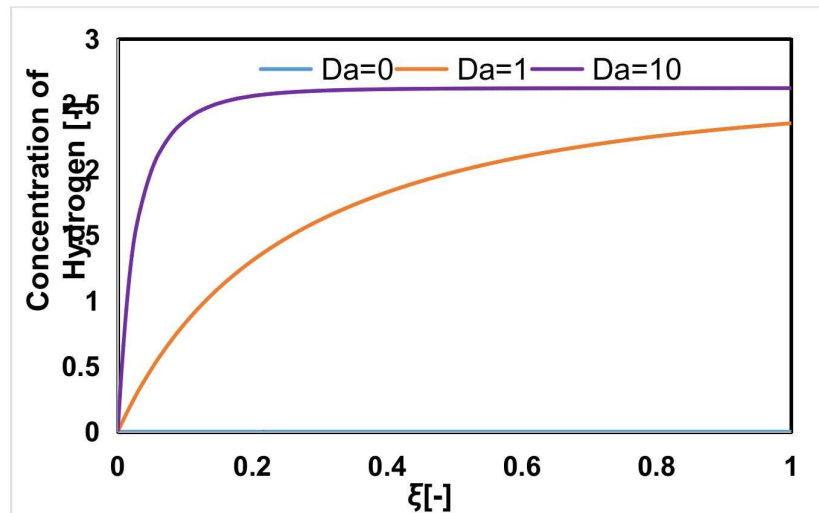


Fig 6: Non-dimensional Concentration vs Non-dimensional Length

## Length

Using non-dimensional analysis, the effect of the Damköhler number (Da) on the ethanol steam reforming system was investigated. The characteristic reaction rate divided by the convective transport rate is known as the Damköhler number. The importance of reaction kinetics over convective transport increases with Da. Due to the system's preference for quick chemical transformation over physical transport, this change raises the ethanol conversion rate. As a result of the sequential reaction network's advancement, hydrogen production also increases. To validate the application of coupled governing equations in the model and to generalize the behavior, the profiles are displayed in a non-dimensional framework. These dimensionless plots show patterns that are consistent with theory, suggesting that the model accurately accounts for the interaction between reaction and transport phenomena. The consistency in the shape and progression of the curves with increasing Da further confirms the accuracy of the simulation setup and the successful integration of chemical kinetics and mass transport.

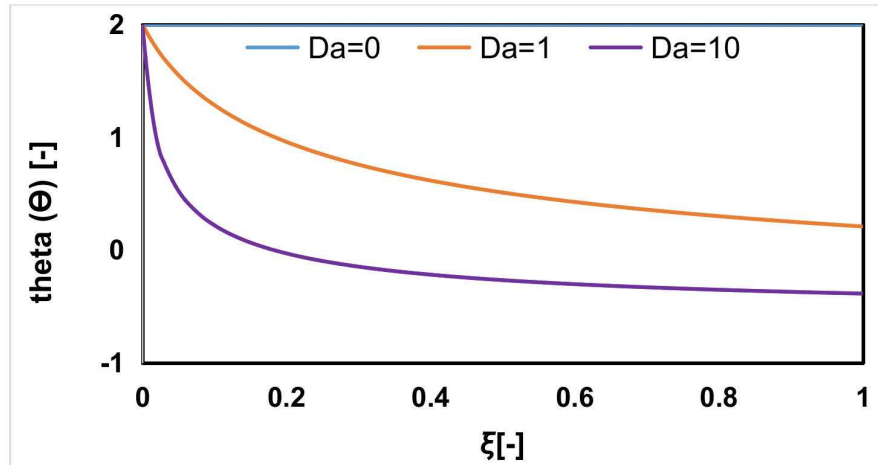


Fig 7: Non-dimensional Temperature vs Non-dimensional Length

An increase in the Damköhler number (Da) reflects a growing dominance of the chemical reaction rate over convective transport within the system. A higher Damköhler number in the context of ethanol steam reforming means that reactions are happening faster than the rate at which species are moving through the reactor. This increased reaction activity leads to higher thermal energy consumption because the reforming process is highly endothermic. Because of the absorption of heat needed to maintain the reaction, the local temperature inside the reactor tends to drop as Da increases.

The observed patterns in temperature and concentration profiles are consistent with theory, suggesting that the applied model effectively depicts the interaction of convective heat transfer, reaction kinetics, and convective transport. The robustness of the simulation and the

accuracy of the coupled equations are confirmed by the plots' consistent shape and behaviour across a range of Damköhler numbers.

### Dimensional

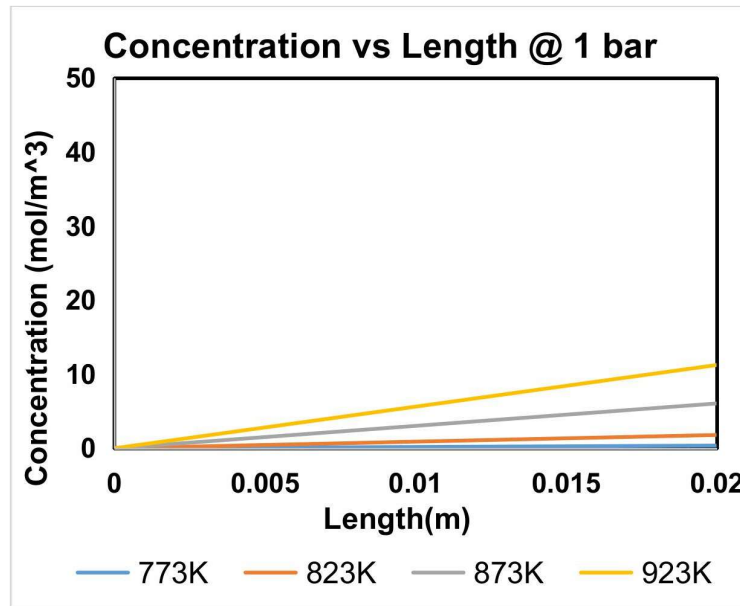


Fig 8: Concentration of Hydrogen vs Length

To investigate the relationship between temperature and hydrogen yield, a parametric analysis was performed. The findings show that the production of hydrogen gradually improves as the temperature rises, peaking at an ideal value beyond which the effect may diminish. This pattern is consistent with endothermic reactions' thermodynamic favorability at high temperatures.

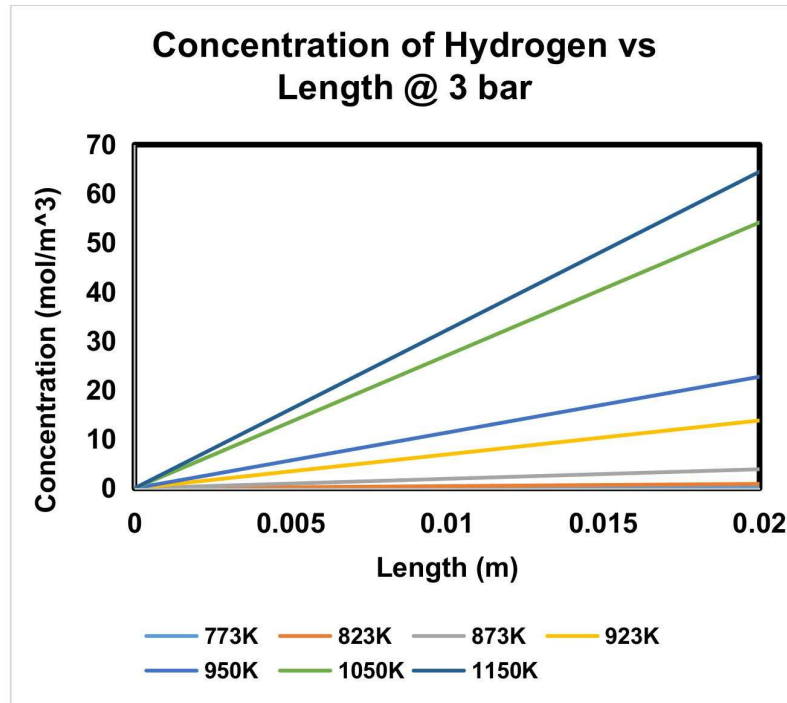


Fig 9: Concentration of Hydrogen vs Length @ 3 bar

Moreover, Figures 8 and 9 illustrate the influence of pressure on hydrogen yield. As pressure increases, a appreciable change in hydrogen production is observed, suggesting that system pressure plays a significant role in promoting reaction efficiency under the given conditions.

## 5.2 Validation of Plots

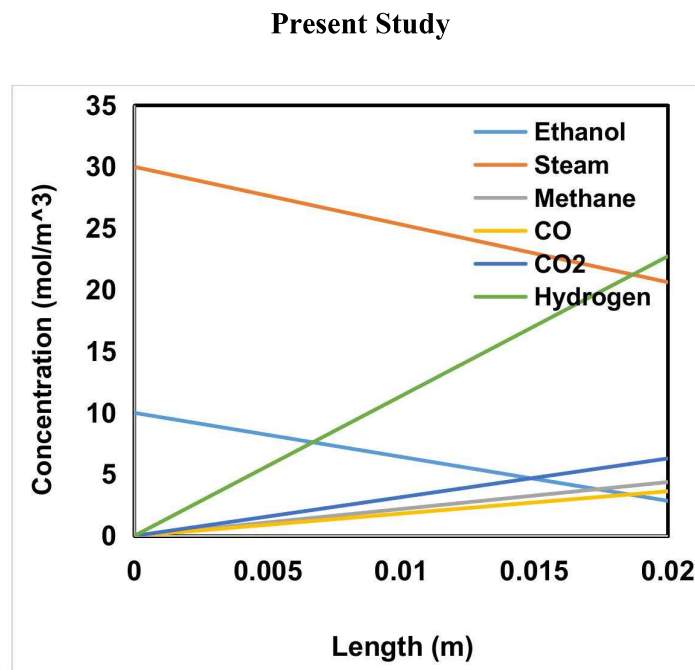


Fig 10: Concentration vs Length @ 950K, 3 bar &

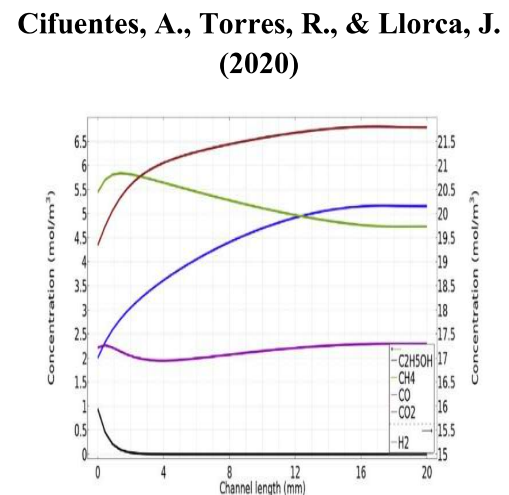


Fig 11: Concentration vs Length @

**S:C =3:1**

**950K, 3 bar & S:C =3:1** (Cifuentes et al., 2020)

The concentrations of different species vary along the reactor's length, as shown in Figure 10. We consulted a published study for validation in order to guarantee the validity of our findings, as illustrated in Figure 11. To allow for a fair comparison, the operating conditions were maintained constant. The outlet concentrations for each of the two studies' participating species are compiled in Table 6. Although the concentration profiles general shapes vary, the final outlet concentrations are fairly similar. The difference in modelling approaches—our model is based on a simplified 1D setup, while the reference study used a 3D honeycomb reactor geometry—is the reason for this variation in trends.

Table 6: Comparison Between reference data and study data

Species	Present study	Cifuentes, A., Torres, R., & Llorca, J. (2020) (Cifuentes et al., 2020)
Ethanol	2.8	Negligible
Steam	20.6	-
CH <sub>4</sub>	4.1	4.7
CO	3.0	2.4
CO <sub>2</sub>	5.7	6.6
H <sub>2</sub>	20.1	20.2

At 1150 K, 4 bar pressure, and a steam-to-carbon ratio of 3:1(Fig. 11), the simulation results demonstrate a peak hydrogen yield of about 80%, which is in close agreement with values

documented in earlier studies. The dependability of our model and the selected operating conditions are supported by this consistency.

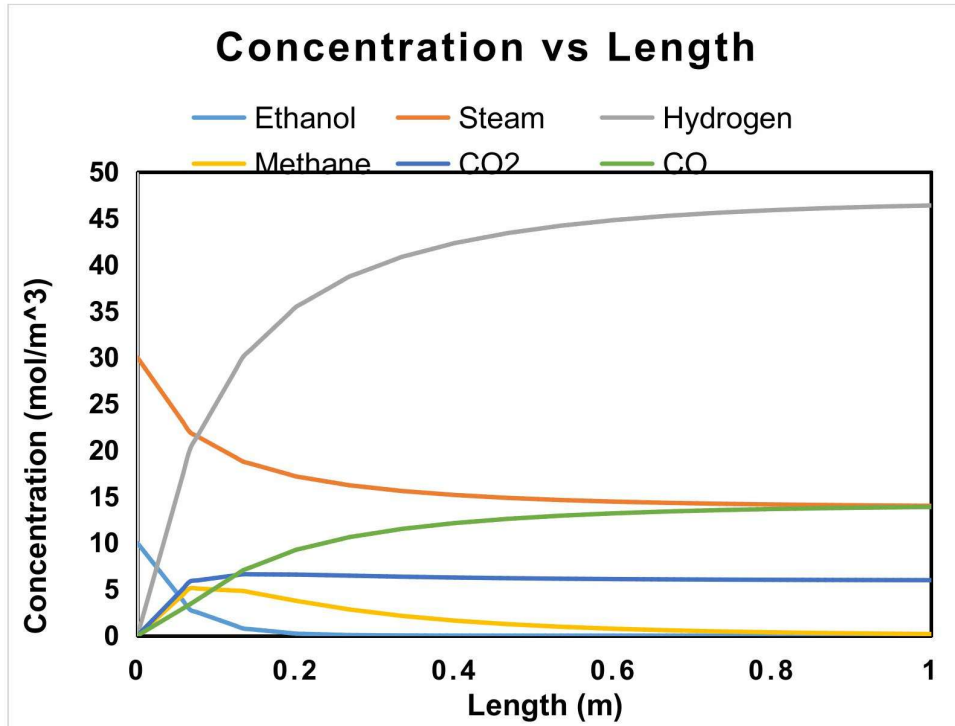


Fig 11: Concentration vs Length @ 1150K, 4 bar and S:C=3:1

### 5.3 Two Dimensional – without heat flux

Initially, plots were created for the process without any heat flux being applied. As anticipated, because the reforming reactions were endothermic, the temperature steadily decreased along the reactor's length. Under these circumstances, ethanol conversion continued to occur, but the system did not produce enough thermal energy to effectively drive the reactions, so the amount of hydrogen produced remained relatively low.

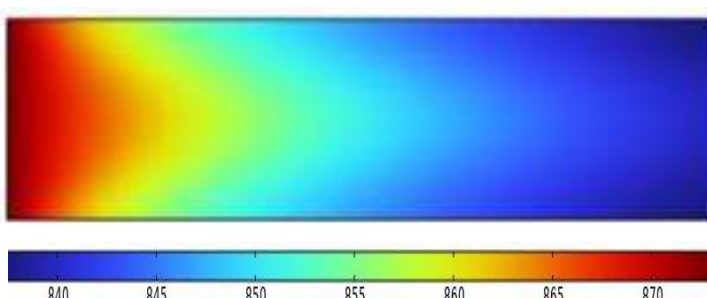
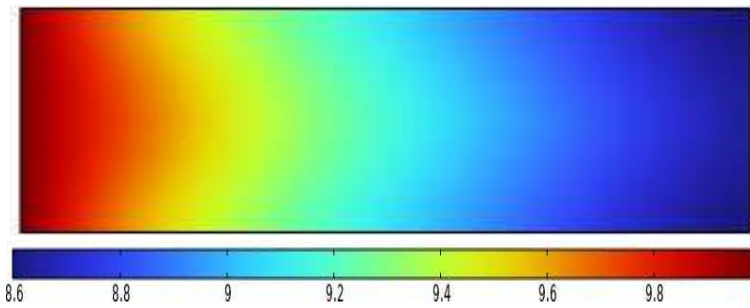
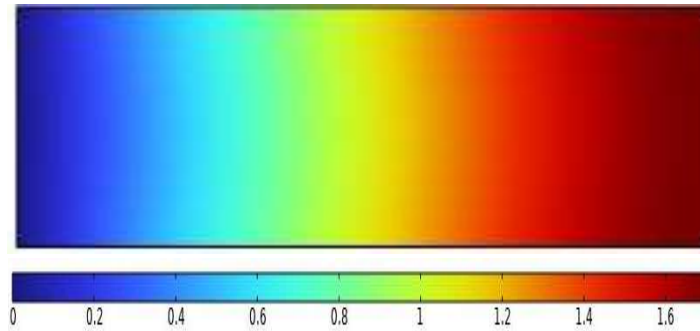


Fig 12: Temperature plot without heat flux



**Fig 13: Ethanol Conversion plot without heat flux**



**Fig 14: Hydrogen Yield plot without heat flux**

#### 5.4 Two Dimensional – with heat flux

The application of heat flux results in a noticeable improvement in ethanol conversion, which raises the yield of hydrogen. The reactions become more favourable as the heat flux intensity rises, leading to increased hydrogen production and ethanol conversion.

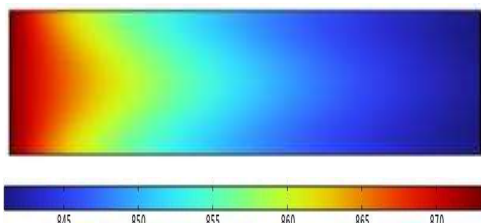


**Fig 15: Temperature plot with heat flux of 100 W/m<sup>2</sup>**

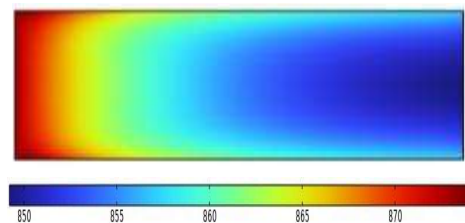


**Fig 16: Temperature plot with heat flux of 500 W/m<sup>2</sup>**

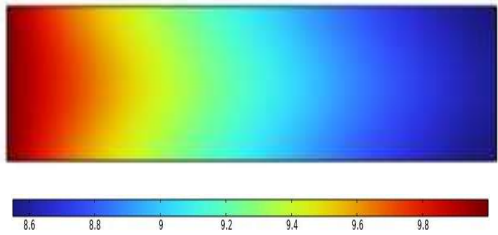


**Fig 17: Ethanol conversion plot with heat flux of  $100 \text{ W/m}^2$**

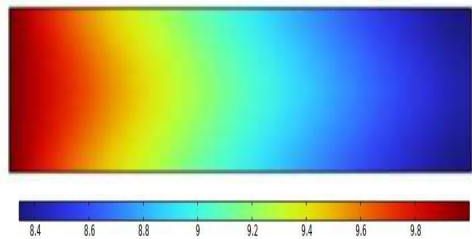


**Fig 18: Ethanol conversion plot with heat flux of  $500 \text{ W/m}^2$**

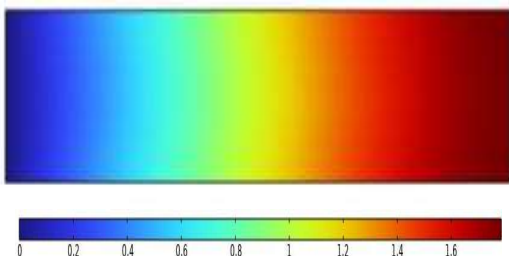


**Fig 19: Hydrogen Yield plot with heat flux of  $100 \text{ W/m}^2$**

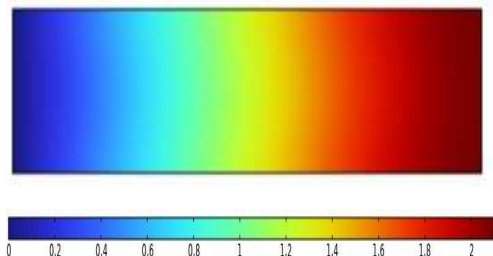


**Fig 20: Hydrogen Yield plot with heat flux of  $500 \text{ W/m}^2$**

## 5.5 Two Dimensional – without ohmic heating

There is no apparent improvement over the situation without any heating when ohmic heating is used without an external heat flux. This suggests that in order to increase hydrogen yield with ohmic heating alone, more optimization is required.

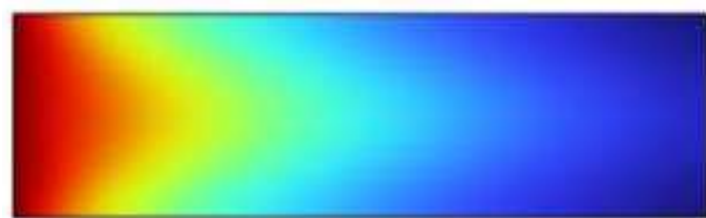




**Fig 21: Temperature plot with ohmic heating**

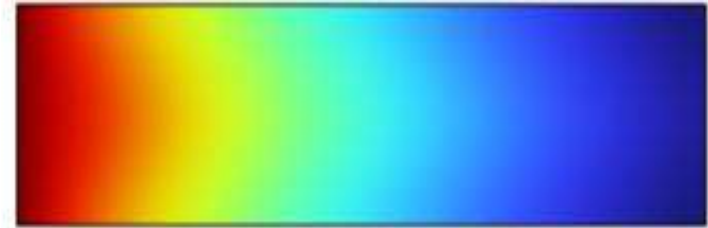


**Fig 22: Ethanol conversion plot with ohmic heating**

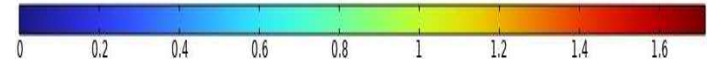
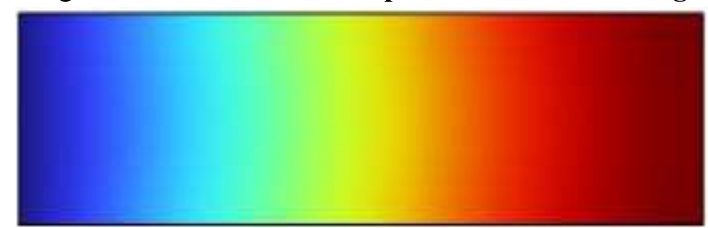


**Fig 23: Hydrogen Yield plot with ohmic heating**

## 6. CONCLUSIONS & FUTURE WORK

This project focused on the modelling and analysis of ethanol steam reforming for hydrogen production, incorporating both kinetic and thermodynamic perspectives. A detailed parametric study was carried out to understand how key variables like temperature and pressure affect hydrogen yield. The findings confirmed that higher temperatures and pressures significantly enhance hydrogen production, consistent with the endothermic nature of the reforming reactions.

To improve process efficiency, the concept of electrification was explored through ohmic heating, inspired by modern energy-efficient approaches. Model validation was performed by comparing our 1D simulation results with data from literature, including a study based on a

3D honeycomb reactor. While some differences were observed in concentration profiles due to geometric variations, the final species concentrations showed good agreement, supporting the accuracy of our model.

Overall, this work demonstrates the potential of using electrically assisted heating methods to optimize hydrogen production from ethanol, opening up new possibilities for cleaner and more efficient fuel generation technologies.

Joule heating can be completely incorporated into the model for upcoming research in order to precisely represent its thermal effects on hydrogen yield and reaction kinetics. Furthermore, a more accurate depiction of flow and heat transfer behaviour will be possible by expanding the simulation to a complete 3D reactor geometry.

## References

- [1] Almind, M. R., Vendelbo, S. B., Hansen, M. F., Vinum, M. G., Frandsen, C., Mortensen, P. M., & Engbæk, J. S. (2020). Improving performance of induction-heated steam methane reforming. *Catalysis Today*, 342, 13–20.  
<https://doi.org/10.1016/j.cattod.2019.05.005>
- [2] *Chapter 4 Coupling of ethanol steam reforming and ethanol combustion: Design driven by CFD Modeling 4.1. Introduction.* (n.d.).
- [3] Cifuentes, A., Torres, R., & Llorca, J. (2020). Modelling of the ethanol steam reforming over Rh-Pd/CeO<sub>2</sub> catalytic wall reactors. *International Journal of Hydrogen Energy*, 45(49), 26265–26273. <https://doi.org/10.1016/j.ijhydene.2019.11.034>
- [4] Sidhu, T. P. K., Govil, A., & Roy, S. (2017). Optimal monolithic configuration for heat integrated ethanol steam reformer. *International Journal of Hydrogen Energy*, 42(12),